JOURNAL OF GEOPHYSICAL RESEARCH, VOL. 103, NO. A5, PAGES 9165–9176, MAY 1, 1998

Structure of the dissipation region during collisionless magnetic reconnection

M. A. Shay and J. F. Drake

Institute for Plasma Research, University of Maryland, College Park

R. E. Denton

Wilder Laboratory, Dartmouth College, Hanover, New Hampshire

D. Biskamp

Max-Planck-Institut für Plasmaphysik, Garching, Germany

Abstract. Collisionless magnetic reconnection is studied using a 2 1/2-dimensional hybrid code including Hall dynamics and electron inertia. The simulations reveal that the dissipation region develops a two-scale structure: an inner electron region and an outer ion region. Close to the X line is a region with a scale of c/ω_{pe}, the electron collisionless skin depth, where the electron flows completely dominate those of the ions and the frozen-in magnetic flux constraint is broken. Outside of this region and encompassing the rest of the dissipation region, which scales like c/ω_{pi}, the ion inertial length, is the Hall region where the electrons are frozen-in to the magnetic field but the ions are not, allowing the two species to flow at different velocities. The decoupling of electron and ion motion in the dissipation region has important implications for the rate of magnetic reconnection in collisionless plasma: the ions are not constrained to flow through the very narrow region where the frozen-in constraint is broken so that ion flux into the dissipation region is large. For the simulations which have been completed to date, the resulting rate of reconnection is a substantial fraction of the Alfvén velocity and is controlled by the ions, not the electrons. The dynamics of the ions is found to be inherently nonfluid-like, with multiple ion beams present both at the X line and at the downstream boundary between the inflow and outflow plasma. The reconnection rate is only slightly affected by the temperature of the inflowing ions and in particular the structure of the dissipation region is controlled by the ion inertial length c/ω_{pi} and not the ion Larmor radius based on the incoming ion temperature.

1. Introduction

Magnetic reconnection plays an important role in the dynamics of the magnetosphere, the Sun, and laboratory fusion experiments. The dissipation region, where the frozen-in flux constraint is broken, controls the rate of reconnection in a resistive magnetohydrodynamic (MHD) description [*Biskamp*, 1986]. At small values of resistivity the dissipation region forms an elongated Sweet-Parker layer and the rate of reconnection is very low, with an inflow velocity v_i into the X line which scales like

$$v_i = \frac{\delta}{\Delta} v_A << v_A \qquad (1)$$

Paper number 97JA03528.
0148-0227/98/97JA-03528$09.00

where δ and Δ are the width (controlled by resistivity) and length (macroscopic) of the dissipation region, respectively, and v_A is the Alfvén velocity. This relation follows from continuity and the Alfvén limit on the ion outflow velocity. In the magnetosphere the classical collision rate is very small and the inertia of electrons allows the frozen-in flux constraint to be broken and magnetic reconnection to proceed [*Vasyliunas*, 1975]. The exploration of the structure of the dissipation region in the collisionless limit and its role in controlling reconnection is critical to the development of an understanding of magnetic reconnection in the magnetosphere.

In a recent two-fluid treatment of collisionless reconnection it was demonstrated that the dissipation region develops a two-scale structure, an inner region of transverse scale size c/ω_{pe} controlled by the electron dynamics embedded in a larger layer of scale length c/ω_{pi} con-

trolled by the ions [*Biskamp et al.*, 1997]. Outside of the dissipation region the electrons and ions move together and both are frozen into the magnetic field. Within a scale length c/ω_{pi} of the neutral line the Hall effect allows the electron and ion motion to decouple, the electrons remaining frozen-in to the magnetic field and the ions being diverted in the direction of the outflow from the neutral line [*Mandt et al.*, 1994; *Biskamp et al.*, 1997]. The electrons continue to accelerate toward the neutral line until they decouple from the magnetic field in a region of scale length c/ω_{pe}. They are then ejected from the neutral line with high velocity, greatly exceeding the Alfvén velocity, and eventually slow and rejoin the ions in the outflow from the dissipation region. An important conclusion from the calculation was that the decoupling of electron and ion motion in the dissipation region greatly enhances the rate of reconnection compared to the rates which would be obtained without this effect. This enhancement can be understood from the expression for the reconnection inflow rate in (1). In the MHD limit the region where the electrons and ions decouple from the magnetic field and the ion outflow channel are the same. In the two-fluid or hybrid description the ions decouple from the electrons and magnetic field on the scale length c/ω_{pi} and the electrons decouple from the magnetic field on the scale c/ω_{pe}. In this non-MHD generalization, (1) describes ion continuity and the region where the ions, and not the electrons, decouple from the magnetic field. The ion dynamics therefore define the scale lengths δ and Δ and $\delta \sim c/\omega_{pi}$. On this basis, (1) implies that the ions and not the electrons control the rate of reconnection, and this was confirmed in the simulations [*Mandt et al.*, 1994; *Biskamp et al.*, 1997]. In the absence of the Hall effect the ions are constrained to follow the electrons down to the scale length c/ω_{pe} so that $\delta \sim c/\omega_{pe}$ and the reconnection rate is dramatically reduced.

Since the ions play the critical role in determining the rate of reconnection, it is important that the ion model include the essential physics required to accurately describe the size scaling of the dissipation region. The description of the electrons may not be as important since their dynamics impacts the rates of reconnection less strongly. In the previous two-fluid treatment [*Biskamp et al.*, 1997], potentially important effects such as the ion current, ion pressure, and compressibility were neglected. In the present paper we extend the previous work by considering a hybrid model in which the ions are modeled as particles and the electrons as a finite mass fluid. We explore the role of the ions in controlling the structure of the dissipation region and rate of magnetic reconnection. We show that the ion dynamics both around the X line and in the outflow region are intrinsically nonfluid-like since the resulting distribution functions consist of multiple beams. The transition region separating the inflow and outflow regions downstream of the neutral line, which is interpreted as a slow shock in the MHD description [*Petchek*, 1964], cannot be interpreted as a simple shock in the hybrid model: high-velocity ions ejected from the vicinity of the X line mix with the plasma flowing directly across the "shock" and prevent the Rankine-Hugoniot conditions from being satisfied. Finally, we explore the scaling of the reconnection rate with the equilibrium scale length L. Over the range of scales which we are able to complete simulations, the rate of reconnection is nearly independent of the macroscale, the inflow velocity being of order $0.1v_A$. However, separation of scales between c/ω_{pi} and L is not yet sufficient to conclude that this rate will remain invariant at larger values of L. Since the treatment of electrons is unchanged from the previous calculations, we do not focus on the role of electrons except to note that, as in the earlier calculations, the rate of reconnection is insensitive to the scale length c/ω_{pe} and therefore to the electron mass even though c/ω_{pe} is required for reconnection to occur.

2. Hybrid Simulation Model

The equations used to complete the simulations are as follows:

$$\frac{\partial \mathbf{B}'}{\partial t} = -\nabla \times \mathbf{E}' \tag{2}$$

$$\mathbf{E}' = \frac{1}{n}\mathbf{J} \times \mathbf{B}' - \frac{1}{n}\mathbf{J}_p \times \mathbf{B} - \frac{1}{n}\nabla P_e \tag{3}$$

$$\mathbf{B}' = (1 - \delta_e^2 \nabla^2)\mathbf{B}, \quad \mathbf{J} = \nabla \times \mathbf{B} \tag{4}$$

$$\frac{\partial P_e}{\partial t} = -\mathbf{u_e} \cdot \nabla P_e - \gamma P_e \nabla \cdot \mathbf{u_e}, \tag{5}$$

where $\gamma = 5/3$, $\mathbf{J}_p = n\mathbf{u}_i$ = ion flux, $\mathbf{u}_e = \frac{1}{n}(\mathbf{J}_p - \mathbf{J})$ = electron flow, P_e = electron pressure, and $\delta_e = c/\omega_{pe}$. Time is normalized to the ion cyclotron time Ω_i^{-1} with B evaluated at its maximum initial value. Length scales are normalized to the ion inertial length, c/ω_{pi}, where n is given by the average of the initial density (nearly constant for the simulations presented here). The velocities therefore are normalized to the Alfvén velocity. We also assume quasi-neutrality: $n_i \approx n_e$. The above equations form a closed set except for $\mathbf{J}_p$ and n, which are calculated by stepping forward the individual ion particles and then projecting the appropriate moments onto the grid. In Ohm's law in (3) the first term after the equal sign produces the Hall effect and introduces the scale length c/ω_{pi} into the equations. This scale does not appear explicitly because it has been absorbed into the normalization. The first and third terms after the equal sign in (3) are absent in MHD. The electron inertia in Ohm's law manifests itself through the term proportional to δ_e^2 in the definition of $\mathbf{B}'$. The inclusion of the electron pressure in the system leads to numerical problems which are eliminated by a small viscosity in (5) and (2). In addition, a sixth-order k space diffusion is added to (2) to eliminate the pile-up of energy at the grid scale.

The equations used to step forward the particles are

$$\frac{d\mathbf{x}_i}{dt} = \mathbf{v}_i, \tag{6}$$

$$\frac{d\mathbf{v}_i}{dt} = \mathbf{E}'' + \mathbf{v}_i \times \mathbf{B}, \tag{7}$$

where $\mathbf{E}'' = -\mathbf{u}_e \times \mathbf{B} - \frac{1}{n}\nabla P_e$. Note that we neglect the finite electron inertial correction to the electric field which is used to step the ions forward in time because this correction only becomes important at spatial scales of c/ω_{pe}. Changes in the electric field over a distance of c/ω_{pe} have very little effect on the motion of the ions because of their large mass. Because whistler waves in the electron fluid have a much higher velocity than waves associated with the ions, the time step for the fluid is taken to be much smaller than that of the ions [*Mandt et al.*, 1994]. For all simulations presented in this paper, the time step for the ions is 0.1 in normalized units and the time step for the electrons is 1/50 that of the ions (typically $0.05\Omega_e$).

The focus of this work is on the structure of the dissipation region during reconnection and not on the initiation of reconnection during substorm onset. For this reason we consider an idealized problem, the merging of two magnetic flux bundles [*Mandt et al.*, 1994; *Biskamp et al.*, 1997] as shown in Figure 1. The net current in each flux bundle is zero so that the bundles are individually in equilibrium and isolated from the boundaries of the simulation. Unlike the case of two simple wires with parallel current, the flux bundles have no net attractive force. To initiate reconnection, the flux bundles are overlapped slightly as shown in Figure 1. The reconnected field lines then drive the flow as in a conventional slab geometry. This flux bundle system has the advantage over conventional slab geometries that the reconnection process does not saturate but continues robustly until the two bundles have completely merged, the reconnection rate being determined entirely by the dynamics of the dissipation region. A more subtle advantage over the slab system is that the displacement of the bundle toward the X line does not distort the magnetic fields in the bundle and therefore does not increase the magnetic energy. That is, it is marginally stable to ideal perturbations and is therefore essentially equivalent to the long-wavelength limit of the tearing mode in a slab system, which also has this property and which is most relevant to magnetic reconnection in the magnetosphere.

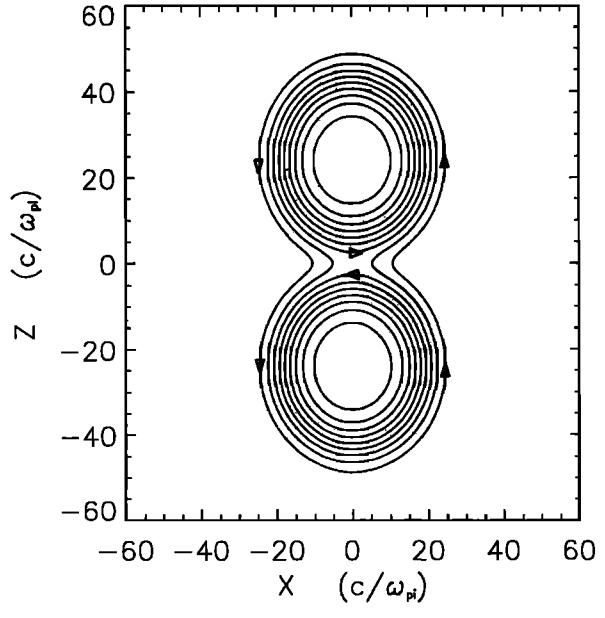

Figure 1. The initial magnetic field and other initial parameters.

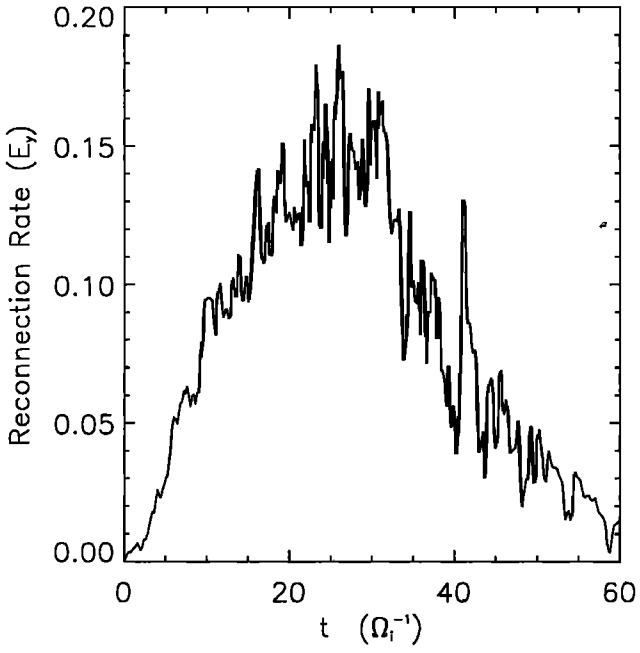

Figure 2. Out of plane electric field at the X line induced by the reconnection process.

The initial magnetic field in each flux bundle is given by $\mathbf{B} = \hat{\mathbf{z}} \times \nabla\psi + B_z\hat{\mathbf{z}}$, where the magnetic flux ψ is given by $\psi_0 e^{-(r/L)^4}$, B_z is a uniform axial magnetic field, L is the radius of the flux bundle, r is the distance from the center of the flux bundle, and ψ_0 is chosen such that the maximum value of the in-plane magnetic field is 1.0. In the simulations discussed in this paper we have taken $B_z = 0.1$ in the initial state with the density constant and the current carried by the electrons. The magnetic pressure, $B^2/2$, is balanced by the magnetic tension and the electron pressure, P_e, allowing the ion temperature T_i to be spatially constant initially. We vary T_i in order to explore its impact on the structure of the dissipation region and the rate of reconnection.

The system has three important spatial scale lengths: c/ω_{pe}, c/ω_{pi}, and the radius of the flux bundles, L. Ideally, $c/\omega_{pe} \ll c/\omega_{pi} \ll L$, because $c/\omega_{pe} \ll c/\omega_{pi}$, and $L \gg c/\omega_{pi}$ in space plasma systems. In the magneto-

tail, for example, $c/\omega_{pi} \sim 0.16R_e$, and $L \gtrsim 5R_e$, with R_e the radius of the Earth so that $L/(c/\omega_{pi}) \gtrsim 30$. Because there are three disparate lengths which must be well separated, this system is computationally challenging to model. Using a 1024×1024 grid and 21 million particles in our largest run allowed us to choose $c/\omega_{pe} = 0.2$ (a mass ratio $m_i/m_e = 25$), and $L = 20$. These numbers provide a sufficient separation of scales to address most but not all of the important physics issues.

3. Simulation Results and Discussion

As the reconnection proceeds, the changing flux at the X line induces an out-of-plane electric field, which is a direct measure of the rate of reconnection. Figure 2 is a plot of this out-of-plane electric field for the case $c/\omega_{pe} = 0.2$, $L = 10$, and $T_i = 0.2$ with a grid scale length of 0.1 in each direction and 20 particles per cell. The reconnection rate quickly increases to about 0.13, remains approximately constant for about 20 time units (ignoring the spikes which are a consequence of wave-induced density fluctuations) and then decreases as the strength of the magnetic field flowing into the X line is reduced. The bundles are almost completely reconnected by $t = 48$. The dissipation region evolves to a quasi-steady state during the interval of maximum reconnection rate. In Figures 3-5 are blowups of some of the important quantities which characterize the dissipation region in this quasi-steady state for a run where $c/\omega_{pe} = 0.2$, $L = 20$, and $T_i = 0.2$. The three scale sizes, c/ω_{pe}, c/ω_{pi}, and L, break the dissipation region into corresponding areas where different physics dominates. This is illustrated in Figure 3 where we show plots of the region where the Hall effect is important (the first term in (3) is comparable to the second), where the electron inertia is important ($\delta_e^2\nabla^2\mathbf{B} \sim \mathbf{B}$) and the corresponding in-plane magnetic field. The Hall region shown in Figure 3a consists of the dissipation region, which is macroscopic along x and several c/ω_{pi} along z, and several wing-like appendages. The smaller wings which map onto the separatrix are associated with outward propagating whistlers. The larger wings, which are downstream of the separatrix, are linked to "slow shocks" which accelerate the ions in the direction of the outflow. In the Hall region the electrons and the ions are decoupled and the electrons remain frozen to the magnetic field. Outside of the Hall region the conventional MHD equations remain valid. The electron inertial region in Figure 3b lies within a distance of around c/ω_{pe} of the X line and extends along the separatrices of the magnetic field. In this region the electrons are no longer frozen into the magnetic field, and magnetic reconnection can take place. We define the dissipation region as those regions near the X line where ideal MHD breaks down, that is, the Hall region (minus the wing-like appendages) and the central electron inertial regions denoted in Figure 3.

The ion and electron flows are shown in Figure 4. The maximum velocity vector in Figure 4a for the ions is 0.65, close to the upstream Alfvén velocity which is ~ 0.8, and in Figure 4b for the electrons is 2.86. The ions flow toward the Hall region with a nearly constant velocity. At a distance of several c/ω_{pi} from the neutral line they turn and flow outward from the neutral line. Their velocity increases with increasing $| x |$ until about $x \approx 10$ and then slowly decreases as the flow begins to diverge. The corresponding electron velocities are shown in Figure 4b. The region of high electron velocity is much more localized around the neutral line than that of the ions. The electrons turn toward the outflow at a distance around c/ω_{pe} from the neutral line and then accelerate outwards, reaching their maximum velocity at $x = 2$. The peak outflow velocity of the electrons is not limited by the Alfvén velocity [*Biskamp et al.*, 1997] and clearly exceeds this limit in Figure 4b. In this inner region therefore the electron velocities greatly exceed those of the ions.

The out-of-plane flows of the electrons and ions and the out-of-plane magnetic field are shown in Figure 5. The ion out-of-plane flow has a width which is several c/ω_{pi} and a length which is macroscopic. The electron out-of-plane flows are strongly peaked around the neutral line and separatrices, mirroring closely the electron inertial region shown in Figure 3b. Since the magnetic field is frozen into the electrons nearly everywhere, the out-of-plane flow of electrons drags the magnetic field in this direction, producing the corresponding out-of-plane field shown in Figure 5c [*Mandt et al.*, 1994]. The electron flows and fields in Figures 5b and 5c produce a standing whistler wave which propagates outward along the magnetic field from the X line. The velocity of the whistler greatly exceeds the Alfvén velocity and therefore the inflow velocity. The whistler disturbance therefore lies very close to the separatrix. The high-velocity electrons flowing toward the neutral line near the separatrix in Figure 4b produce currents which sustain the out-of-plane magnetic field in Figure 5c and are therefore part of the whistler current system. The whistler dynamics are responsible for accelerating the outflowing electrons to high velocity [*Mandt et al.*, 1994; *Biskamp et al.*, 1997].

As discussed previously, the flow into and out of the dissipation region controls the reconnection rate. The scaling of the width and height of the ion flow channel with the important physical scale lengths is therefore important. We define a rectangle of width δ and length Δ whose ends are the values of x where the outflow is a maximum and whose width is defined so that 70% of the ion outflow is passing through the ends of the rectangle at this value of x. The reconnection rate is insensitive to c/ω_{pe}, as noted earlier. We also find that the reconnection rate is insensitive to the ion Larmor radius, ρ_i (to be discussed later). The scaling of the reconnection rate with the flux bundle size, L (the only remaining free parameter), is therefore of primary in-

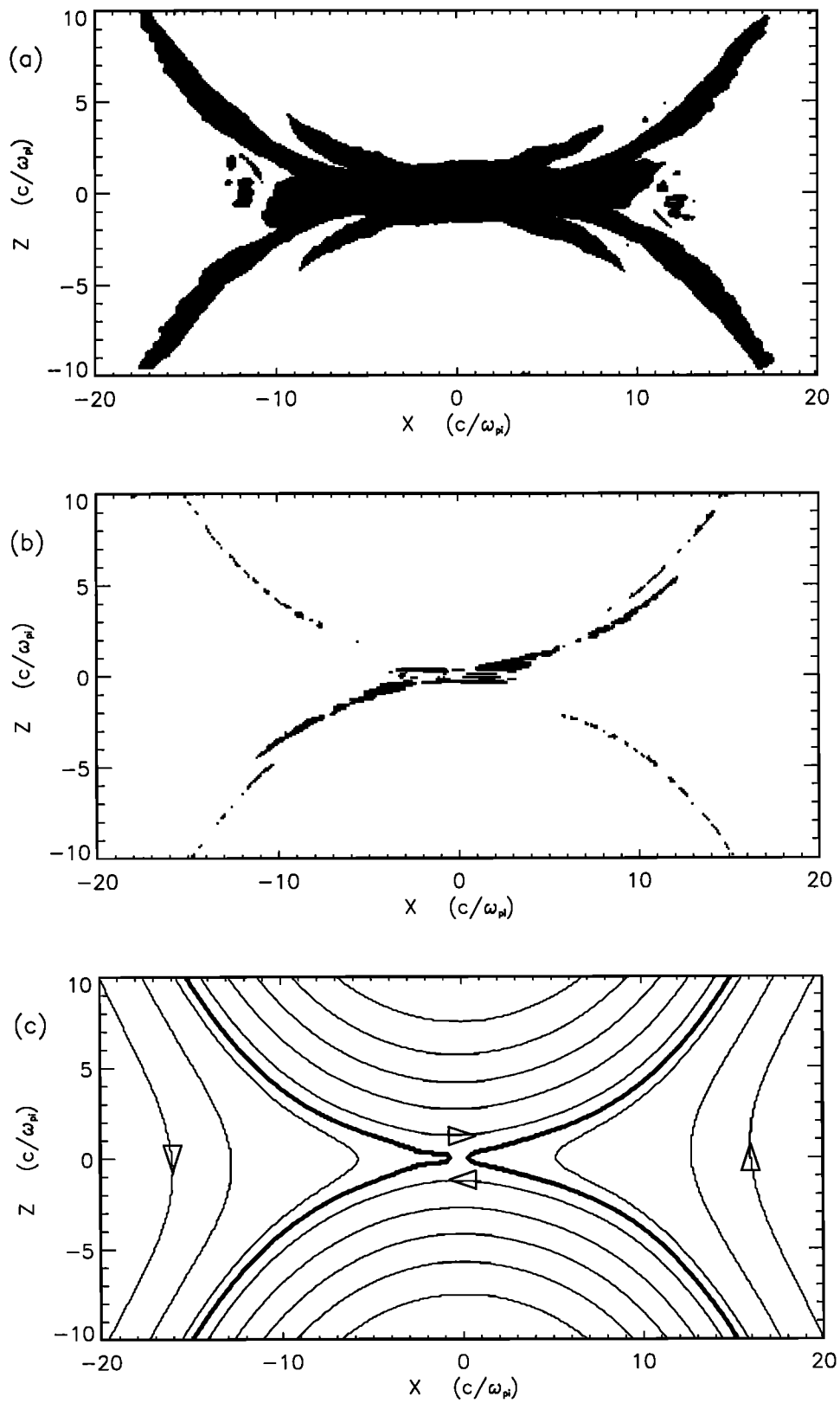

Figure 3. (a) The Hall region: those areas where $\mathbf{J} \times \mathbf{B}' \geq 1/4(\mathbf{J_p} \times \mathbf{B})$ for at least one component, (b) the electron inertial region: those areas where $\delta_e^2 \nabla^2 \mathbf{B} \geq 1/4\mathbf{B}$ for at least one component, and (c) the magnetic field. The thick line in Figure 3c is the separatrix.

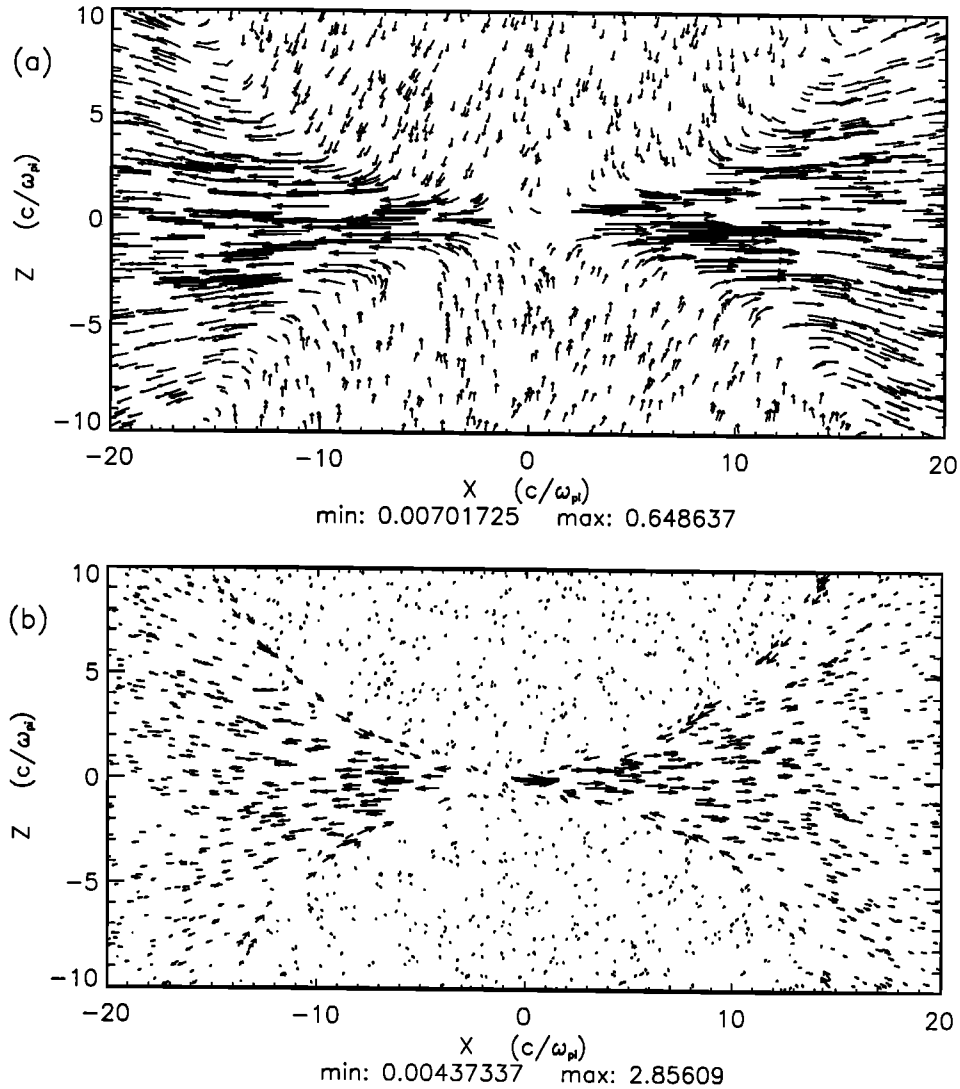

Figure 4. The (a) ion and (b) electron flows at the same time as in Figure 3 with the minimum and maximum values.

terest. Figure 6 is a plot of the inflow v_i and outflow v_o velocities and scale lengths δ and Δ versus L. In a near steady state the ion fluxes into and out of the dissipation region must be equal, that is, $v_i\Delta = v_o\delta$. This condition is satisfied within about 10% for the numbers given in Figure 6. While δ is independent of L, Δ is proportional to L for the range of values explored. The ion dissipation region and current layer therefore scale like c/ω_{pi} (or perhaps ρ_i which was a constant in Figure 6). This scaling is consistent with recent laboratory experiments of magnetic reconnection [*Yamada et al.*, 1996]. The inflow velocity v_i, which is a measure of the rate of reconnection, is constant, while v_o increases with L. The maximum ion outflow velocity v_m is also plotted in Figure 6a. Figure 6 implies that the reconnection inflow velocity is a constant $\approx 0.1v_A$, independent of L. However, the scaling shown in Figure 6 cannot continue at larger values of L because v_o would exceed the Alfvén speed, which is of order unity in normalized units. In fact, in Figure 6a the maximum ion outflow speed is essentially equal to the Alfvén speed at the largest value of L. At larger L, v_o must approach a constant and either v_i must decrease, lowering the reconnection rate, or Δ must stop increasing with L. Based on the present simulations, the rate of reconnection at larger values of L cannot be predicted.

Up to this point we have not discussed the impact of finite T_i on the rate of reconnection or the structure of the ion flow layer. Raising T_i effectively increases the ion Larmor radius ρ_i compared with the ion skin depth c/ω_{pi}. For the parameters of Figures 3-5, $\rho_i \sim 0.6c/\omega_{pi}$. The effect of T_i on the reconnection process is small, but discernable. As T_i is increased from 0.0 to 0.2, the time for the flux bundles to completely reconnect increases by 20%. Above $T_i = 0.2$, however, the total reconnection time is independent of T_i. Even for $T_i = 0$ the basic structure of the flows is unchanged in Figures 4a and 5a. The reason for this will be clearer once we dis-

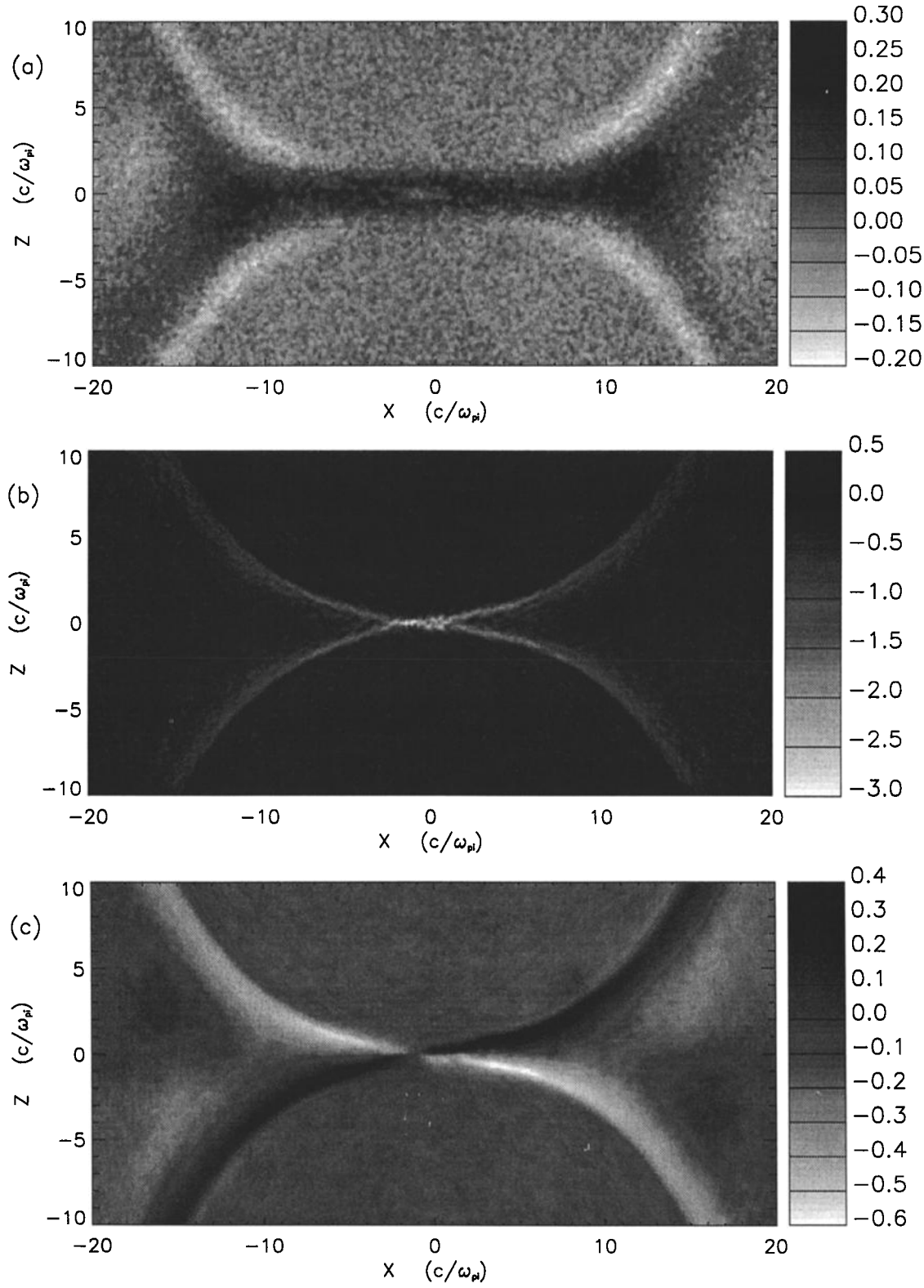

Figure 5. Out-of-plane (a) ion flow, (b) electron flow, and (c) magnetic field.

cuss the ion dynamics close to the X line in more detail. Thus it is c/ω_{pi} and not ρ_i which controls the widths of the layers. For ρ_i greater than c/ω_{pi} the ion velocity and current layers tend to be smoothed by ρ_i, but the reconnection rate is unchanged.

The structure of the electron current layer has previously been discussed in some detail in earlier work [*Biskamp et al.*, 1997], and therefore we have not focused on this topic. Nevertheless, it is useful to note some differences between the structure of the electron

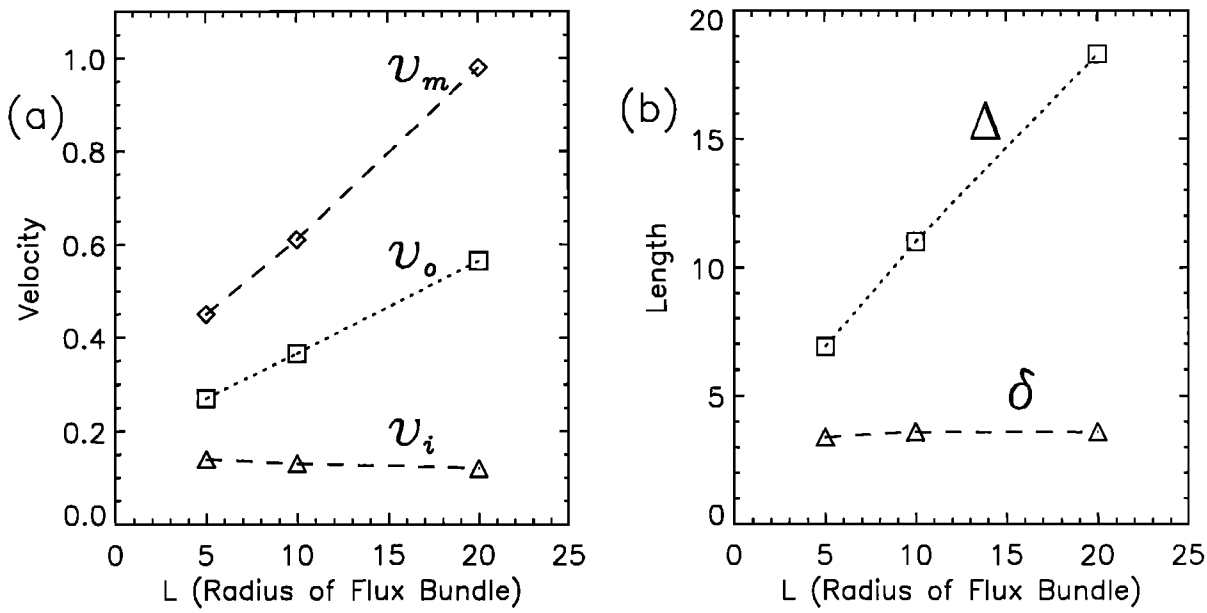

Figure 6. Scaling of the dissipation region with the bundle radius: (a) average ion outflow velocity v_o, maximum ion outflow velocity v_m, and inflow velocity v_i and (b) width δ and length Δ of the dissipation region.

and ion layers. As in the case of the ions, one can define characteristic lengths and widths of the electron layer and associated inflow and outflow velocities and examine their scaling. The most significant difference between the electron and ion layers is the length, which is macroscopic in the case of the ions and is microscopic (in the sense that its length tends to zero in the limit $c/\omega_{pe} \rightarrow 0$) in the case of the electrons. In the case of the electrons the integrated current across the layer tends to zero as $c/\omega_{pe} \rightarrow 0$, and the electrons therefore can not modify the magnetic field enough to form a macroscopic current layer. In the absence of an out-of-plane guide field, the electrons simply can not carry very much current across **B**. The integrated ion current across the layer by contrast remains finite even as $c/\omega_{pi}/L$ becomes very small, and the ions are therefore able to form a macroscopic current sheet. The absence of a macroscopic electron current sheet is a primary reason why the electrons do not limit the rate of reconnection.

As discussed in earlier hybrid simulations of magnetic reconnection [*Krauss-Varban and Omidi*, 1995; *Nakabayashi and Machida*, 1997], the ion distribution function can develop multiple beams as streams of ions penetrate one another. Under such circumstances a fluid treatment becomes problematic. In the present simulations, multiple beam distributions become very prominent both close to the X line and in the outflow region just downstream of the separatrix. The ions $\mathbf{E} \times \mathbf{B}$ drift toward the dissipation region with a nearly constant velocity around 0.15. Close to the X line, the ions are accelerated inwards by a large, localized electric field E_z which is shown in Figure 7a along with the corresponding magnetic field B_x. This electric field develops in the Hall region, where the ions are unmagnetized, to force the ions to follow the electrons which $\mathbf{E} \times \mathbf{B}$ with increasing velocity towards $z = 0$. The ions are accelerated toward the midplane ($z \approx 0$) near the X line by this electric field to a velocity ≈ 0.7. After crossing the midplane, the ions are turned around by B_x and E_z and are accelerated out of the plane by the reconnection electric field E_y. The orbit of an ion moving in the magnetic and the electric fields given in Figure 7a and a constant reconnection electric field in the y direction of $+0.13$ is shown in Figure 7b. Its turning points for the first few oscillations are around $z \approx \pm 0.7$. The maximum velocity along $\hat{\mathbf{y}}$ occurs at the turning points and is around 0.7. The maximum velocity along $\hat{\mathbf{z}}$ occurs at $z = 0$ and is about ± 0.7. Thus, assuming that a large number of particles flow into the reconnection region from both sides, we would expect to see counterstreaming particles at $(x, z) = (0, 0)$ with average velocities along $\hat{\mathbf{z}}$ of 0.7. Also, since the maximum velocity along $\hat{\mathbf{y}}$ occurs at the turning points, we would expect the maximum out-of-plane ion flow to occur at around $z \approx 0.7$. Figure 7c is the ion distribution function $f(v_z)$, integrated over v_x and v_y at $(x, z) = (0, 0)$, from the simulation in Figures 3-6. Note the two peaks at $v_z \approx \pm 0.5$, which is consistent with the counterstreaming ions predicted from Figure 7b. Figure 7d is a cut along z of the out-of-plane ion flow along $\hat{\mathbf{y}}$ at $x = 0$. Note the double peaks at $z \approx \pm 0.6$, which is consistent with the calculated turning points at $z \approx \pm 0.7$. From the observational perspective it is important to note that the velocities of the counterstreaming beams in Figures 7c and 7d greatly exceed the ambient inflow velocity which

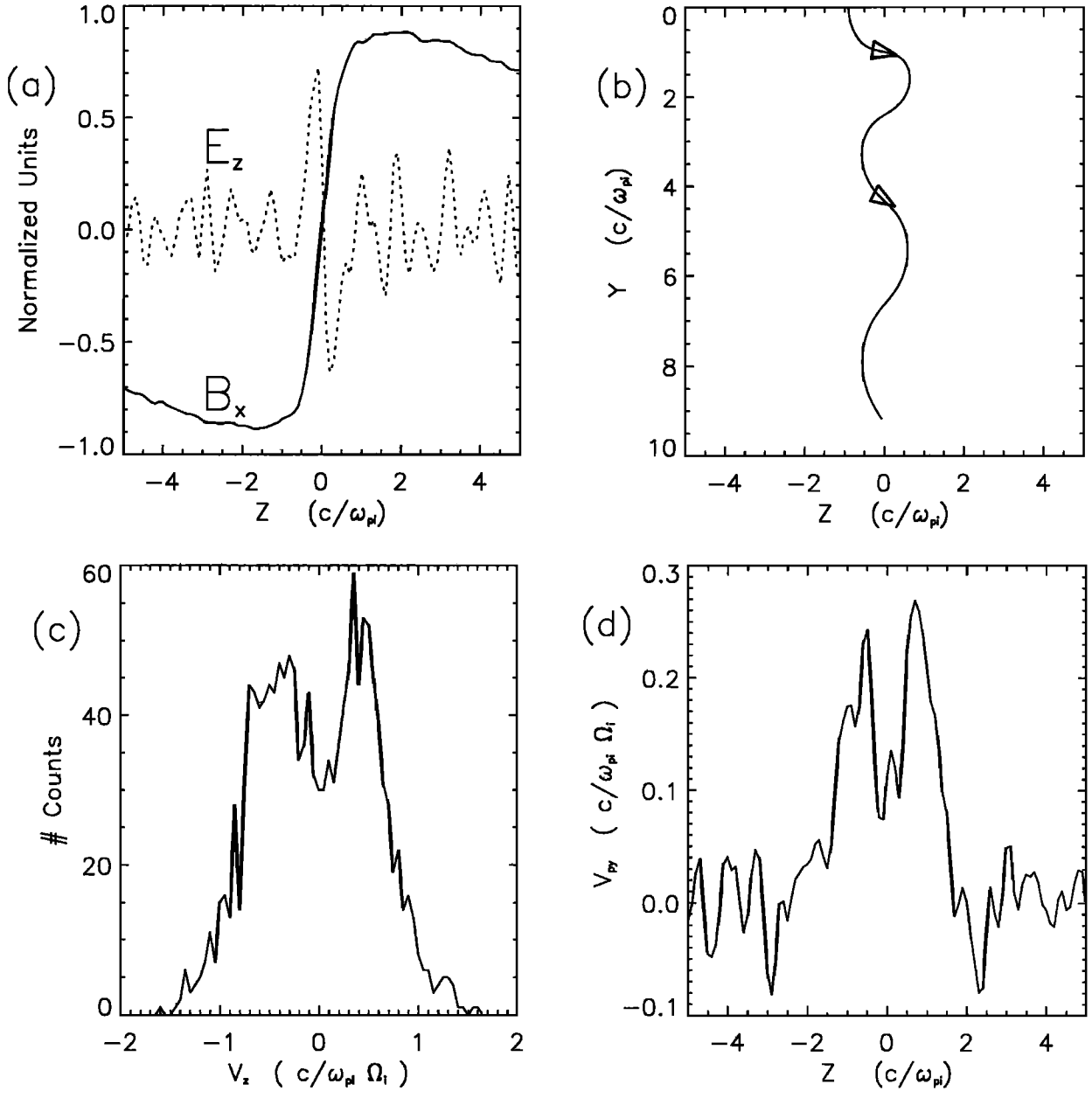

Figure 7. Nonfluid-like structures of ions around X line: (a) E_z and B_x versus z at $x = 0$, (b) trajectory of average ion particle at $x = 0$, (c) distribution function at $(x, z) = (0, 0)$ integrated over v_x and v_y, and (d) out-of-plane ion velocity, v_{py}, at $x = 0$.

characterizes the larger-scale ion dissipation region (see Figure 6a) and in fact are comparable to the Alfvén velocity. The beam velocities are the order of or greater than the local ion thermal velocity and should be easily measureable if a satellite is very close to the X line.

Thus the acceleration of the ions into the dissipation region is due to electric fields associated with the high-speed flows of the electrons in this region. The same process accelerates the ions out of the dissipation region. The electrons are accelerated to high velocities (exceeding the Alfvén velocity) toward and then away from the X line. Because the ions are much more massive, they cannot keep up with the electrons and a separation between the two species occurs which produces electric fields which point toward the midplane in the inflow region near the X line and away from the X line in the outflow region. In the dissipation region it is this electric field, and not the magnetic field, which accelerates the ions toward the X line and then to Alfvén speeds away from the X line.

The longer wing-like appendages which appear in the Hall region of Figure 3a are associated with "slow shocks" [*Coroniti*, 1971] which abruptly turn the inflowing ions toward the outflow (see Figure 4a). Fig-

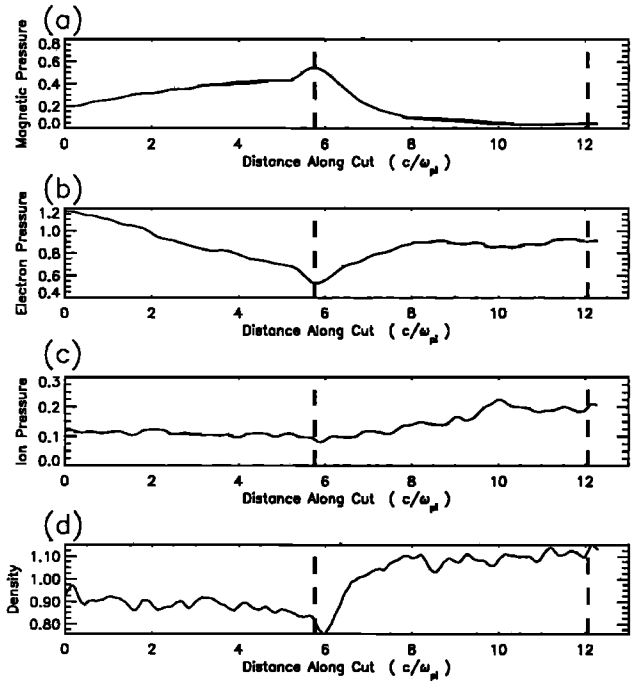

Figure 8. (a) Magnetic pressure, (b) electron pressure, (c) ion pressure, and (d) density along a cut perpendicular to the "slow shock" from the simulation shown in Figure 3. The vertical dashed lines mark the positions of the separatrix and the $z = 0$ symmetry line, respectively. The cut crosses the magnetic separatrix in Figure 3 at $x, z = 10.6, 4.8$.

ure 8 shows the variation of the magnetic pressure, the electron pressure, the ion pressure, and the density in the direction perpendicular to the "slow shock" from the simulation shown in Figures 3-5. The vertical dashed lines give the location of the separatrix and the location of the $z = 0$ symmetry line. The cut crosses the magnetic separatrix in Figure 3c at $x, z = 10.6, 4.8$. As expected from a slow shock, the magnetic pressure drops sharply and the electron pressure and density rise rapidly (over a scale length of around $2c/\omega_{pi}$) such that the total pressure is nearly constant in moving from the inflow to the outflow side of the discontinuity. The ion pressure changes only over a longer scale length (of order $4c/\omega_{pi}$). There are a number of features of this "slow shock" which do not match the conventional wisdom. First, the discontinuity clearly begins very close to the separatrix, apparently initiated by the electron currents which map out from the X line along the field lines. The rise in the ion pressure further downstream from the separatrix is in better agreement with the MHD description [*Petchek,* 1964]. There is also no traveling wave train structure downstream of the shock as predicted in fluid theory (see Figure 5c) [*Coroniti,* 1971].

The integrated force parallel to the discontinuity is also not consistent with the measured change in the corresponding ion flow across the discontinuity. Downstream of the discontinuity, the flow parallel to the "shock" is too large when compared to the integrated force. The failure of this Rankine-Hugoniot condition is due to nonlocal acceleration of the ions. While some of the outward flowing ions just downstream of the discontinuity have been accelerated by the "shock," others have passed through the dissipation region where they were accelerated by large electric fields associated with the fast electron flows. These two acceleration processes lead to two separate species of ions just downstream of the "shock:" a background, slow moving species that has been accelerated by the discontinuities in the magnetic field across the "shock," and a high-speed beam which has been accelerated by the large electric fields near the X line. These two species can be clearly seen in the distribution function of the ions from the downstream region shown in Figure 9a. The slow-moving ions appear as a Gaussian distribution centered around a velocity of $v_x = 0.2$ and $v_z = -0.2$. The distribution of the faster species has a kidney bean-like shape with an axis of symmetry along the magnetic field line (the direction of the arrow in Figure 9a). There are approximately twice as many slow ions as there are fast ions. Such distribution functions have been widely observed in the plasma sheet boundary layer and have been interpreted as arising from magnetic reconnection [*Birn et al.,* 1981]. Figure 9b shows the spatial location of the particles which make up the distribution in Figure 9a. It is superimposed on a plot of the out-of-plane current so that its location compared with the discontinuity in the magnetic field can be easily seen. In Figure 9c we show the location of these same ions at an earlier time. Note that the ions come from two separate locations, one straddling the discontinuity at positive z and the other below the X line. The slow-flowing background ions come primarily from above the discontinuity, and the fast beam comes from the population near the X line. The mixing of the two distinct species from different regions of space implies that the traditional MHD treatment of the slow shock is not valid, and the associated Rankine-Hugoniot jump conditions are not satisfied. Thus the discontinuities which appear downstream of the X line are not true slow shocks.

4. Conclusions

In conclusion, we find that the dissipation region has a two-scale structure associated with the electron and ion scales c/ω_{pe} and c/ω_{pi}. This two-scale structure allows the ions, and not the electrons, to control the rate of reconnection in collisionless plasma. For all of the values of $L/(c/\omega_{pi})$ examined in this study, the reconnection rate was found to be Alfvénic with an inflow velocity of approximately $0.1v_A$. The Hall effect, which allows electron and ion motion to decouple in the dissipation region, and therefore allows the width of the ion outflow channel from the dissipation region to scale like c/ω_{pi} rather than an electron scale, is essential for achieving fast reconnection. The behavior of the ions

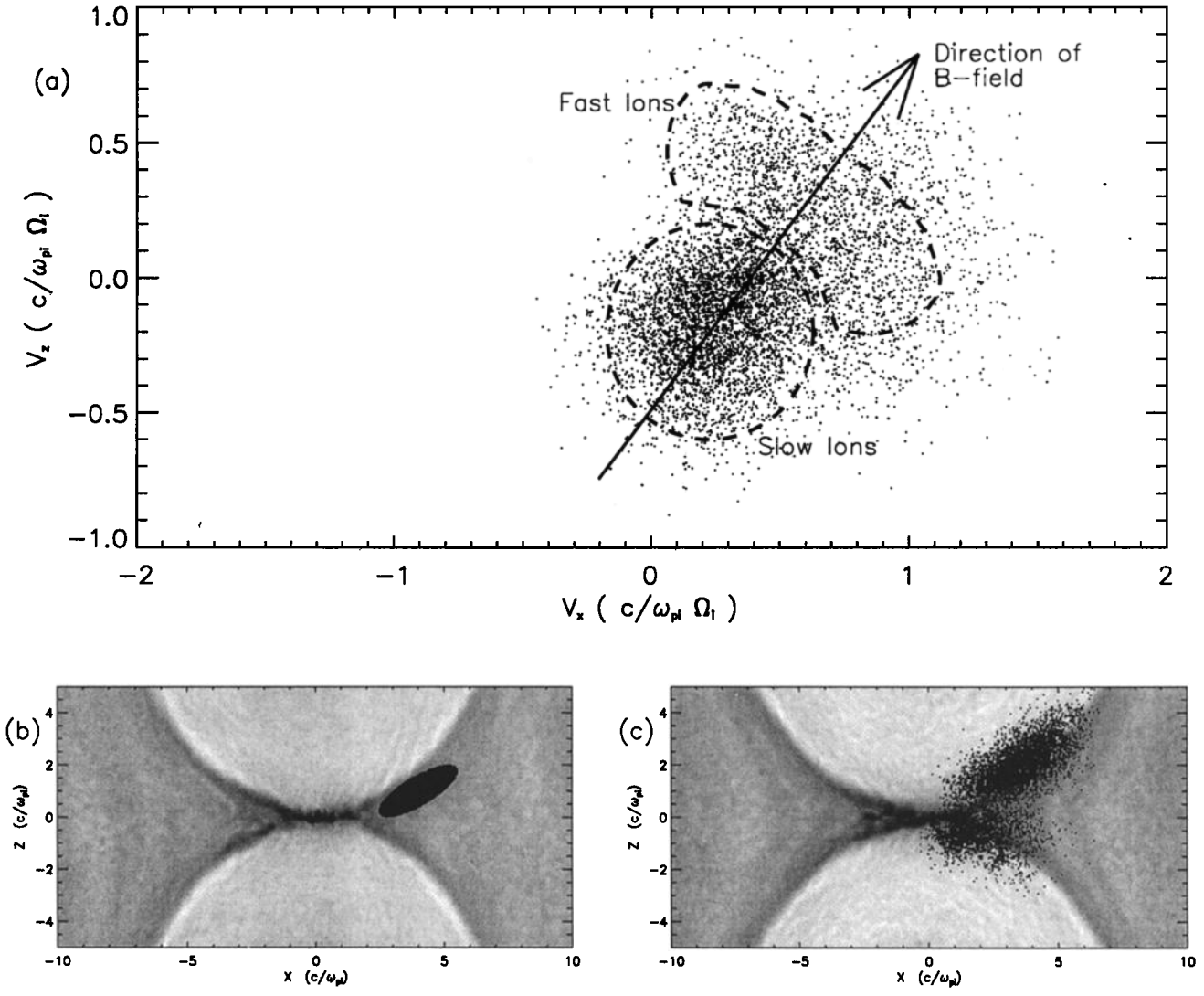

Figure 9. (a) Scatterplots of ion in-plane velocities, (b) location of particles from Figure 9a, and (c) the location of the same particles at an earlier time.

inside the dissipation region is decidedly nonfluid-like because of counterstreaming and nonlocal acceleration effects.

The reconnection rates found are consistent with timescales associated with the release of magnetic energy stored in the lobes during the expansion phase of substorms. Taking a lobe density of $0.05/\text{cm}^3$, $B \sim$ 15 nT, we calculate that $v_A = 1500$ km/s and that the inflow velocity into the X line is of order 150 km/s. In 10 min a significant fraction of the lobe flux can be reconnected.

A number of issues remain to be resolved even in the context of collisionless magnetic reconnection in the two-dimensional limit. Simulations of magnetic reconnection with a full particle code indicate that the transverse scale length of the electron current layer is controlled by the thermal motion of electrons rather than electron inertia [*Horiuchi and Sato,* 1997] in the case where the equilibrium out-of-plane magnetic field is small. Hybrid simulations using a full tensor to model electron pressure evolution also indicate that electron thermal motion can control the structure of the electron current layer [*Hesse and Winske,* 1993; *Kuznetsova and Hesse,* 1998]. Thus futher investigations of the structure of the inner electron layer with a more complete model than that presented here are warranted. The scaling of the rate of reconnection when macroscopic scale lengths are very large compared with c/ω_{pi} remains an important issue especially for understanding reconnection in the solar corona. Finally, in three dimensions there is evidence that narrow electron layers break up [*Drake et. al.,* 1994, 1997]. Thus it seems likely that the intense current layers localized around the X line and extending along the separatrices in Figure 5b will not survive in the physical system.

Acknowledgments. We would like to thank M. Hesse, M. Kuznetsova, and A. T. Y. Lui for valuable discussions.

This work was supported by NSF grant ATM-9625242 and by NASA grant NAGW-5175.

The Editor thanks D. Winske and another referee for their assistance in evaluating this paper.

References

Birn, J., T. G. Forbes, E. W. Hones Jr., and S. J. Bame, On the velocity distribution of ion jets during substorn recovery, *J. Geophys. Res.*, *86*, 9001, 1981.

Biskamp, D., Magnetic reconnection via current sheets, *Phys. Fluids, 29*, 1520, 1986.

Biskamp, D., E. Schwarz, and J. F. Drake, Two-fluid theory of collisionless magnetic reconnection, *Phys. Plasmas, 4*, 1002, 1997.

Coroniti, F. V., Laminar wave-train structure of collisionless magnetic slow shocks, *Nucl. Fusion, 11*, 261, 1971.

Drake, J. F., R. G. Kleva, and M. E. Mandt, The structure of thin current layers: Implications for magnetic reconnection, *Phys. Rev. Lett., 73*, 1251, 1994.

Drake, J. F., D. Biskamp, and A. Zeiler, Breakup of the electron current layer during 3-D collisionless magnetic reconnection, *Geophys. Res. Lett., 24* , 2921, 1997.

Hesse, M., and D. Winske, Hybrid simulations of collisionless ion tearing, *Geophys. Res. Lett., 20*, 1207, 1993.

Horiuchi, R., and T. Sato, Particle simulation study of collisionless driven reconnection in a sheared magnetic field, *Phys. Plasmas, 4*, 277, 1997.

Krauss-Varban, D., and N. Omidi, Large-scale hybrid simulations of the magnetotail during reconnection, *Geophys. Res. Lett., 22*, 3271, 1995.

Kuznetsova, M. M., and M. Hesse, Kinetic quasi-viscous and bulk flow inertia effects in collisionless magnetotail reconnection, *J. Geophys. Res., 103*, 199, 1998.

Mandt, M. E., R. E. Denton, and J. F. Drake, Transition to whistler mediated magnetic reconnection, *Geophys. Res. Lett., 21*, 73, 1994.

Nakabayashi, J., and S. Machida, Electromagnetic hybrid-code simulation of magnetic reconnection: Velocity distribution functions of accelerated ions, *Geophys. Res. Lett., 24*, 1339, 1997.

Petchek, H. E., Magnetic field annihilation, in *AAS/NASA Symposium on the Physics of Solar Flares*, edited by W. N. Ness, p.425, NASA, Washington, D. C., 1964.

Vasyliunas, V. M., Theoretical models of magnetic field line merging, *Rev. Geophys., 13*, 303, 1975.

Yamada, M., H. Ji, S. C. Hsu, T. A. Carter, R. Kulsrud, and D. Uzdensky, The magnetic reconnection experiment (MRX), *Bull. Am. Phys. Soc., 41*, 1370, 1996.

D. Biskamp, Max-Planck-Institut für Plasmaphysik, 85748 Garching, Germany

R. E. Denton, 6127 Wilder Laboratory, Dartmouth College, Hanover, NH 03755-3528

J. F. Drake and M. A. Shay, Institute for Plasma Research, Energy Research Building 223, University of Maryland, College Park, MD 20742-3511 (e-mail: drake@glue.umd.edu; shay@glue.umd.edu)

(Received August 27, 1997; revised November 24, 1997; accepted December 1, 1997.)